Special Collection

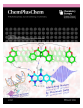

Photocatalytic Oxidative [2+2] Cycloelimination Reactions with Flavinium Salts: Mechanistic Study and Influence of the Catalyst Structure

Tomáš Hartman,[a] Martina Reisnerová,[a] Josef Chudoba,[b] Eva Svobodová,[a] Nataliya Archipowa,[c] Roger Jan Kutta,*[d] and Radek Cibulka*[a]

Dedicated to Professor František Liška on the occasion of his 80th birthday.

Flavinium salts are frequently used in organocatalysis but their application in photoredox catalysis has not been systematically investigated to date. We synthesized a series of 5-ethyl-1,3-dimethylalloxazinium salts with different substituents in the positions 7 and 8 and investigated their application in light-dependent oxidative cycloelimination of cyclobutanes. Detailed mechanistic investigations with a coumarin dimer as a model substrate reveal that the reaction preferentially occurs *via* the triplet-born radical pair after electron transfer from the substrate to the triplet state of an alloxazinium salt. The very photostable 7,8-dimethoxy derivative is a superior catalyst with a sufficiently high oxidation power ($E^* = 2.26$ V) allowing the conversion of various cyclobutanes (with E_{ox} up to 2.05 V) in high yields. Even compounds such as all-*trans* dimethyl 3,4-bis (4-methoxyphenyl)cyclobutane-1,2-dicarboxylate can be converted, whose opening requires a high activation energy due to a missing pre-activation caused by bulky adjacent substituents in *cis*-position.

Introduction

Photolyases are photoenzymes that are common in all kingdoms of life repairing photo-damaged DNA.[1] Photo-damaged DNA typically consists of cyclobutanes arising from [2+2] cycloadditions after UV light absorption. This damage is reversed by light-induced [2+2] cycloeliminations *via* excited fully reduced and deprotonated flavins. Cycloelimination reaction of cyclobutanes resulting in their corresponding alkenes ([2+2] cycloelimination, [2+2] cycloreversion) has been a subject of several theoretical investigations.[2,3] In principle, [2+2] cycloeliminations are forbidden in the ground state.[4] However, a few thermally activated processes have been described for specifically substituted cyclobutanes having strain energy originating from their four ring structure (*ca.* 109 kJ mol^{-1}; ref.[5]) increased by steric effects of substituents.[6] Recently, the use of cyclobutane ring opening has been intensively studied in mechanochemistry.[7] Examples demonstrating the usefulness of [2+2] cycloeliminations in organic synthesis have also been reported.[8]

In the excited state, cyclobutanes open without a significant activation barrier. However, excitation typically requires UV light even when it occurs *via* sensitization.[2] The splitting of a thymine dimer or 1,2-diphenylcyclobutane utilizing cyanoarenes and UV light (313 or 366 nm) is proposed to occur *via* electron-transfer in an exciplex formed between an excited photocatalyst and a substrate.[9] Some [2+2] cycloeliminations based on photoredox catalysis employing a dye and light in the visible spectral range have also been reported: splitting of quinolone and coumarin dimers mediated by pyrylium and trityl salts,[10] cycloreversion of tetraphenylcyclobutanes or triphenyloxetane with (thia)pyrylium salts,[11] and thymine dimer opening by riboflavin tetraacetate (**1**) occurring in the presence of perchloric acid.[12] These systems work *via* oxidative cleavage starting with an electron transfer from a dimer to an excited dye thus differing from the process in flavin-dependent photolyases which is initiated by the cyclobutane reduction.[1a,13]

Recently, we have shown that flavin-based photooxidative splitting is more robust when using the flavinium salt **2b** (Figure 1b) instead of **1** with perchloric or trifluoromethane sulfonic acid (Figure 1a).[14] Because of the positive charge, flavinium salts are strong enough to initiate the oxidative cycloelimination of substrates with high oxidation potentials

[a] Dr. T. Hartman, M. Reisnerová, Dr. E. Svobodová, Prof. Dr. R. Cibulka
Department of Organic Chemistry
University of Chemistry and Technology, Prague
Technická 5, 166 28, Prague 6 (Czech Republic)
E-mail: cibulkar@vscht.cz
[b] Dr. J. Chudoba
Central Laboratories
University of Chemistry and Technology, Prague
Technická 5, 166 28, Prague 6 (Czech Republic)
[c] Dr. N. Archipowa
Manchester Institute of Biotechnology and School of Chemistry
The University of Manchester
Manchester M1 7DN (United Kingdom)
[d] Dr. R. J. Kutta
Institute of Physical and Theoretical Chemistry
University of Regensburg
93040 Regensburg (Germany)
E-mail: roger-jan.kutta@chemie.uni-regensburg.de

Supporting information for this article is available on the WWW under https://doi.org/10.1002/cplu.202000767

This article is part of a Special Collection on "Chemistry in the Czech Republic".

© 2020 The Authors. ChemPlusChem published by Wiley-VCH GmbH. This is an open access article under the terms of the Creative Commons Attribution Non-Commercial NoDerivs License, which permits use and distribution in any medium, provided the original work is properly cited, the use is non-commercial and no modifications or adaptations are made.

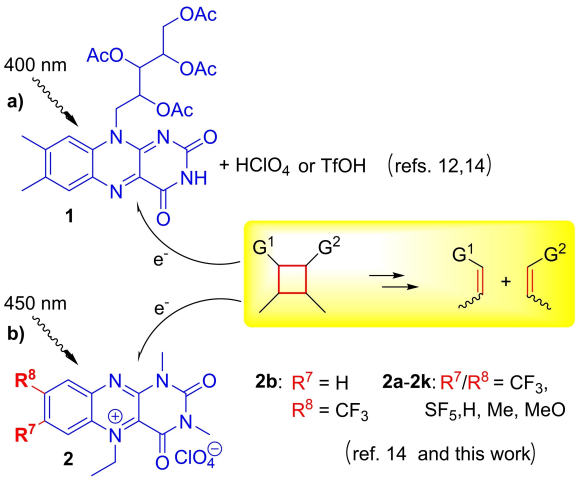

Figure 1. Systems for oxidative [2 + 2] cycloelimination reactions mediated by flavin photocatalysts that are excited by light.

even under neutral conditions. This allowed the extension of the substrate scope demonstrating that the [2 + 2] cycloelimination is a valuable tool in organic synthesis.

In contrast to neutral flavins,[15,16] flavinium salts are novel in photo-redox catalysis.[17] However, application of flavinium salts in "dark" organo-catalysis has been known for several decades.[18] Flavinium salts are mainly used in monooxygenation reactions where they act *via* flavin hydroperoxides analogously to flavin-dependent monooxygenases.[19] In this area, the structure of the flavinium catalyst is crucial for its activity.[20] However, a deep knowledge of the structure to activity relationship is completely missing among flavinium photocatalysts. Herein, following our preliminary results, we report a mechanistic investigation on the [2 + 2] cycloelimination reaction mediated by the excited flavinium salt **2b**. Further, we have prepared a series of flavinium salts **2** in order to study the influence of substitution on their photocatalytic efficiency. We figured out some disadvantages of catalyst **2b**, *e.g.* low activity for less strained substrates. This allowed us the development of a robust and general flavinium-based light-driven procedure for [2 + 2] cycloeliminations.

Results and Discussion

Efficient cycloelimination mediated by 2b

The photocatalytic cycloelimination reaction of **3a** with the flavinium salt **2b** is quantitative within 10 minutes of irradiation at 450 nm light.[14] It is proposed to occur by photoinduced electron transfer (PET) from a substrate to **2b** in an excited state. This proposal was based on i) quenching experiments of the **2b** fluorescence with the coumarin dimer **3a** and ii) the free Gibbs energy for PET, which is −0.51 eV for **3a** at maximum (assuming the S_1 state of **2b** is involved; $E_{red}^{S1}(\mathbf{2b}) = 2.56$ V). Herein, we studied the photocatalytic cleavage of the coumarin dimer **3a** to **4a** by **2b** (Scheme 1) in more detail.

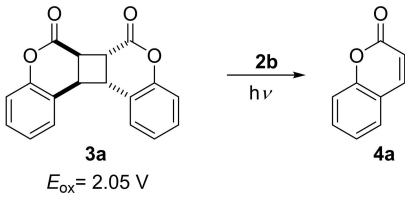

Scheme 1. [2 + 2] Cycloelimination with a model substrate **3a**.

Photo-physics and -chemistry of 2b

First, the photo-physics of **2b** in acetonitrile was investigated by time-resolved absorption spectroscopy (Figure 2a). Importantly, **2b** exists in an equilibrium to its pseudo-base **2b**–**OH** with a pK_{R+} value of 4.8 in water (see Figure 3c).[20a] The formation of **2b**–**OH** depends on the moisture inside the system and it is manifested by an absorption spectrum with a first absorption maximum at 350 nm (see ESI). The formation of **2b**–**OH** is suppressed in the presence of an acid, *e.g.* TfOH or AcOH. Nevertheless, the pseudo-base does not absorb at 450 nm allowing for a selective excitation of only **2b**.

2b shows comparable photo-physics as observed for isoalloxazines. The excitation of **2b** initially leads to the excited singlet state of **2b**, which converts with a lifetime of 4.8 ns partially back to the ground state and partially into the triplet state. The spectra of the S_1 and the T_1 states are very similar to those known for isoalloxazines.[21] The excited singlet state fluorescence quantum yield is determined to $\Phi_{fl} = 11\,\%$ and the triplet yield is determined to *ca.* 89 % (this value was obtained from spectra modelling, see ESI). With a lifetime of 425 ns in non-degassed acetonitrile, the triplet state returns back to the ground state *via* back inter system crossing and energy transfer quenching with molecular oxygen (Figure 2a,c).

Mechanism of the cycloelimination of 3a mediated by 2b

Transient absorption (TA) spectra of **2b** in the presence of **3a** show that the excited states react with the substrate seen in reduced lifetimes and formation of new absorption features (Figure 2b–d). At a concentration of 10 mM of **3a** the excited singlet state lifetime of **2b** is quenched from 4.8 to 3.4 ns giving a bi-molecular quenching rate of $^1k_{eT} = 8.6 \cdot 10^9$ $M^{-1}s^{-1}$. However, corresponding spectral features of the potential radical pair are not observed, indicating that the singlet-born radical pair $^1[\mathbf{2b}^{\bullet(+)}:\mathbf{3a}^{\bullet+}]$ recombines faster than it is formed ending in a non-productive reaction. The T_1 state lifetime of **2b** is also quenched in the presence of 10 mM **3a** from 425 ns to 170 ns giving a bi-molecular quenching rate of $^3k_{eT} = 3.5 \cdot 10^8$ $M^{-1}s^{-1}$. In this case, a triplet-born radical pair $^3[\mathbf{2b}^{\bullet(+)}:\mathbf{3a}^{\bullet+}]$ is formed which is spin-forbidden for recombination, thus, allowing its detection. The triplet-born radical spectrum consists mainly of contributions of the protonated $^2\mathbf{2b}^{\bullet+}$ species (see absorption band at *ca.* 400 nm in Figure 2 and the theoretically calculated absorption spectrum in Figure S18 in the Supporting Information) since the decay of the $^2\mathbf{3a}^{\bullet+}$ is in the order of magnitude

© 2020 The Authors. ChemPlusChem published by Wiley-VCH GmbH

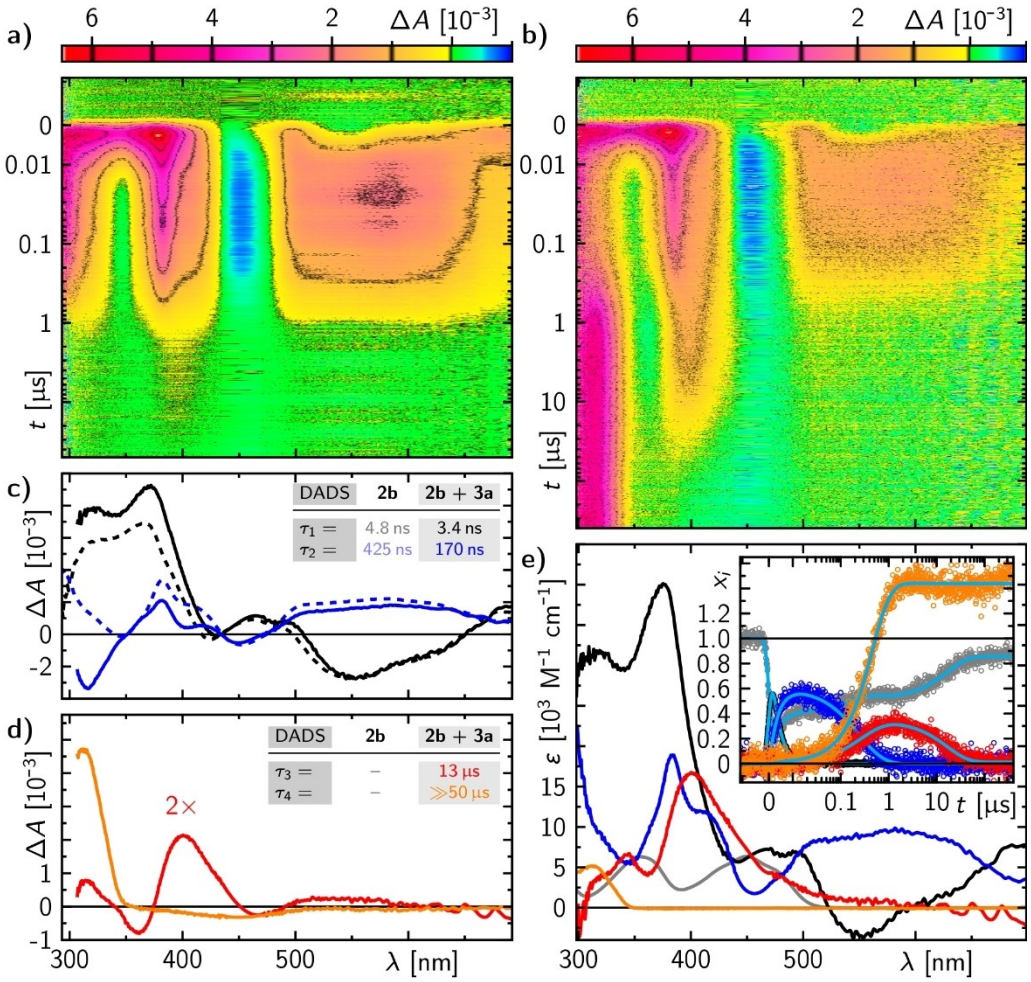

Figure 2. Transient absorption data of **2b** (303 µM) in acetonitrile in the absence (**a**) and presence (**b**) of 10 mM **3a**. **a**,**b**: False colour representation of the transient absorption data. **c**,**d**: Decay associated difference spectra (DADS) resulting from global fits on the data in **a** and **b** with corresponding lifetimes as indicated by the tables in the inset. **e**: Species associated spectra and corresponding concentration time profiles in the inset: grey = **2b** ground state (S_0), black = ^{1}**2b*** excited singlet state (S_1), blue = ^{3}**2b** triplet state (T_1), red = ^{2}**2b**$^{\bullet}$, orange = **4a** product, cyan = global fit. The mole fraction for **4a** is scaled by 0.5 since one **3a** decomposes into two **4a** molecules.

of its formation so that ^{2}**3a**$^{\bullet+}$ does not accumulate to a detectable level. The protonation arises potentially from the moisture in the solvent (to note, the residual water content is expected to be lower in the preparative cycloeliminations. Thus, participation of the neutral radical ^{2}**2b**$^{\bullet}$ under these conditions cannot be excluded). The yield of the triplet-born radical pair can be determined to 60% *via* $\Phi_{eT} = 1 - k_0/k_q$, where k_0 is the total decay rate constant of the triplet in the absence and k_q in the presence of **3a**. Simultaneously with the formation of the triplet-born radical pair another species is formed. Its spectrum has a single absorption band in the detection window peaking at 310 nm and can be assigned to the final product of the cycloelimination **4a** as confirmed by UV/Vis and ^{1}H NMR absorption spectra of pure **4a** (orange spectrum in Figure 2e). On time scales longer than 400 µs the ground state bleach is still observed. *Ca.* 10% of the initially excited molecules **2b** photo-degrade by dealkylation to form **5b** (Scheme 2), which is not resolved in these data. This will be discussed in more detail below. The formed ^{2}**2b**$^{\bullet+}$ that reacts with molecular oxygen

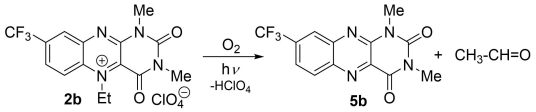

Scheme 2. Light induced dealkylation of **2b**.

(O_2) recovering **2b** and not forming any further **4a** represents a pure loss channel in terms of the total conversion. This is further confirmed by a significantly enhanced quantum yield for this system in the absence of O_2 (see Table S2) so that ^{2}**2b**$^{\bullet+}$ is oxidized back to **2b** by ^{2}**4a**$^{\bullet+}$ forming more **4a**. All known spectra identified and determined in other experiments, *i.e.* the **2b** ground state, the ^{1}**2b*** excited singlet state, the ^{3}**2b** triplet state, the ^{2}**2b**$^{\bullet+}$ radical cation, and the **4a** photo-cleaved final product, allow a perfect decomposition of the transient absorption data into physically meaningful concentration-time profiles as shown in the inset of Figure 2e. As evident the build-up of the product **4a** shows a mole fraction of *ca.* 1.4 indicating a partial radical chain reaction after initial eT under the

© 2020 The Authors. ChemPlusChem published by Wiley-VCH GmbH

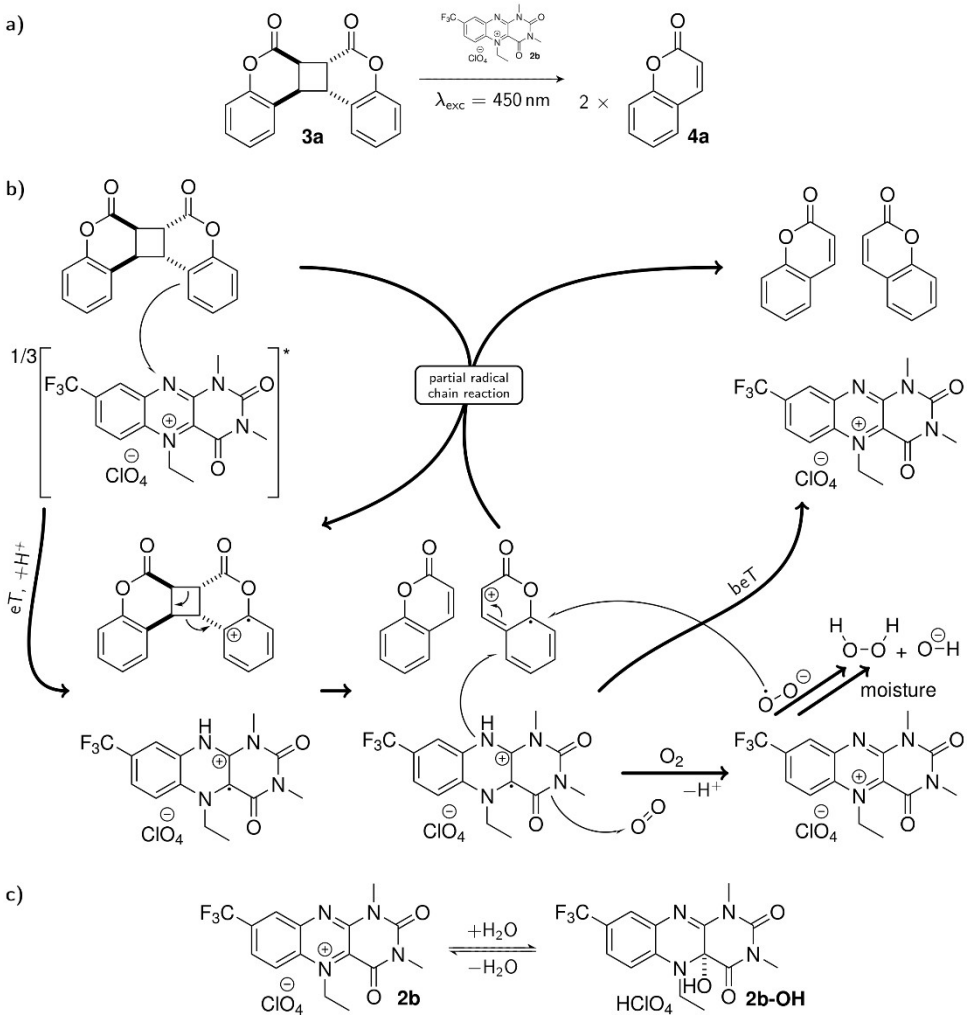

Figure 3. Photocatalytic cleavage of the coumarin dimer **3a** by the excited flavinium salt **2b** to the corresponding coumarin monomer **4a**. General scheme (**a**), reaction mechanism based on time-resolved spectroscopic studies (**b**) and alloxazinium salt **2b**/pseudobase **2b**–**OH** equilibrium with a pK_{R+} of 4.8 in water (**c**).

concentration conditions used in the TA experiment (In comparison to conditions used for the data presented in Table 1, the photocatalyst concentration was 4.6 times higher in the TA experiment). At this point it should be pointed out that the quantum yield of the system is significantly dependent on the concentrations of the participating components (see Table 1). Figure 3 summarizes the proposed reaction mechanism.

Table 1. Comparison of cycloelimination reaction of **3a** to **4a** with **2b** and **5b**.[a]

Catalyst	E_{red}^{S1}[b] [V]	λ_{exc} [nm]	Time [min]	Yield [%][c]	Quantum yield Φ[d]	
					5 mM **3a**	10 mM **3a**
2b	2.56	450	10	quant.	0.31 (0.75)	0.47
5b	2.37	400	60	18	0.003	0.006

[a] Reaction conditions: **3a** (0.02 mmol), **2b** or **5b** (2.5 mol-%), acetonitrile (V = 1 mL), room temperature, under Ar atmosphere. [b] See next section for the determination. [c] Yields determined by ^{1}H NMR. [d] Determined with 66 µM photocatalyst and 5 mM or 10 mM **3a** in non-degassed acetonitrile with expected $c(O_2)$ = 2.4 mM[22] or in degassed acetonitrile by cycles of freeze, pump thaw at a vacuum of 10^{-6} mbar (value in brackets).

Photostability of 2b

The photostability of **2b** was investigated by recording sequences of absorption spectra after a single blue light pulse, or with continuous illumination. When **2b** is illuminated by a single blue light pulse, $\mathbf{2b}^{\bullet+}$ is formed. **2b** partially recovers on a minute time scale, but, interestingly, the recovery is not complete. On prolonged illumination, $\mathbf{2b}^{\bullet+}$ decomposes further into another species with an absorption spectrum peaking at *ca.* 310 and 380 nm, while the latter absorption band shows vibrational fine structure (Figure 4). This photo conversion is entirely irreversible. The ^{1}H NMR of this photo-product reveals that **2b** decomposes upon illumination mainly *via* de-alkylation to alloxazine **5b** and acetaldehyde (Scheme 2; see ESI). The absorption spectrum of pure **5b** is in good agreement with the obtained spectrum of the photo-product of **2b** (Figure 4e,f).

© 2020 The Authors. ChemPlusChem published by Wiley-VCH GmbH

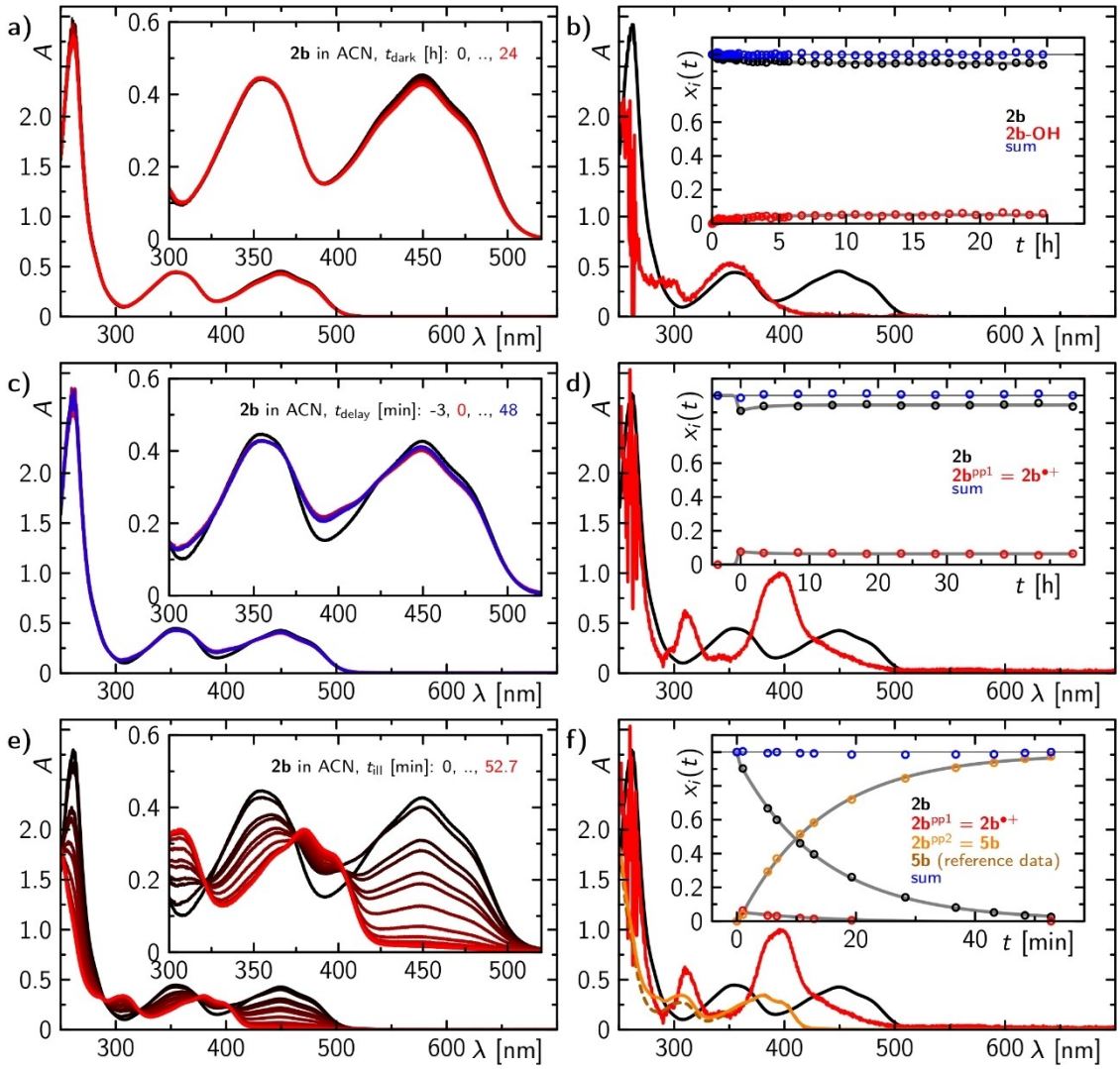

Figure 4. Sequence of stationary absorption spectra and the corresponding concentration-time profiles of formed species, when **2b** dissolved in acetonitrile is either incubated in the dark (**a**–**b**), illuminated by one blue light pulse ($\Delta t = 1$ s; $\lambda_{max} = 450$ nm; **c**–**d**), or stepwise illuminated with blue light ($\lambda_{max} = 450$ nm; **e**–**f**).

Contribution of 5b in cycloeliminations mediated by 2b

Under the conditions used in the preparative cycloelimination reaction with **2b**, the neutral alloxazine **5b** (formed by dealkylation), does not decompose significantly, which raised the question, whether **5b** could also contribute to the cycloelimination. Considering the redox potentials of excited **5b** (2.37 V in maximum) and ground state **3a**, the electron transfer should be energetically allowed. And indeed, using **5b** under otherwise identical reaction conditions resulted in 18% of cycloelimination of **3a** after 60 minutes of irradiation at 400 nm. However, using **5b** as photocatalyst is significantly less efficient than using **2b** which gives quantitative conversion within 10 minutes of irradiation at 450 nm.[14] Further, the determination of the quantum yields for the corresponding cycloelimination using either **2b** or **5b** as photocatalyst in non-degassed acetonitrile (Table 1) reveal that the conversion is by 2 orders of magnitude smaller for **5b** compared to **2b** at a substrate concentration of 5 mM. Thus, under the preparative condition with reaction times on the minutes scale using **2b**, the contribution of **5b** can be neglected. However, for cyclobutane substrates with less steric hindrance, the conversion efficiency might be significantly lower so that longer irradiation times may be required. Therefore, in such cases the efficiency of the cycloelimination will be mainly controlled by **5b**.

Synthesis

The instability observed for **2b** started our search for more suitable alloxazinium catalysts. In order to study a relationship between the structure and the corresponding activity in the series of alloxazinium salts **2**, we prepared a 7-trifluoromethyl derivative **2a** – regioisomer of the originally tested 8-trifluoromethyl salt **2b**. With the aim to introduce a heavy atom into the alloxazine core, we prepared a pair of SF_5-substituted

© 2020 The Authors. ChemPlusChem published by Wiley-VCH GmbH

derivatives **2c** and **2d**. Then, we synthesized an unsubstituted derivative **2e** and a series of methyl- and methoxy- substituted alloxazinium salts **2f**–**k** as representatives of alloxazines with electron-donating group(s) (see Scheme 3 for the structures).

Alloxazinium salts **2** were prepared from the corresponding alloxazines **5** *via* reductive alkylation into position 5 using acetaldehyde followed by oxidation of the flavin skeleton with sodium nitrite (Scheme 3a). In contrast to literature reports,[18a,20a, 23] the reductive alkylation step was performed in dichloromethane providing good yields of the salts **2** (38–74%). Two approaches were applied to synthesize alloxazines **5**. The first approach (Scheme 3b) utilized the condensation of alloxan with an aromatic diamine **6**, readily available from the corresponding nitroanilines **7** *via* reduction. The condensation reaction provided a mixture of 7- and 8- substituted alloxazines **8**, which were alkylated and then separated.

Since the mixture of isomers **5f** and **5g** obtained *via* the first approach could not be separated, an alternative method using anilino uracils **9** prepared from 6-chlorouracil and 3- or 4-methylaniline was used (Scheme 3c). Anilino uracil **9a** was cyclized to alloxazines using oxidative nitrosation with sodium nitrite in acetic acid[24] yielding a mixture of 7-methylalloxazine (**8f**) and 7-methylalloxazine-*N*-oxide (**10a**) which was immediately alkylated using methyl iodide to get a mixture of 1,3,7-trimethylalloxazine (**5f**) and 1,3,7-trimethylalloxazine-*N*-oxide (**11a**) in a moderate yield. The mixture was reduced using H_2/Pd to **5f**. Cyclization of **9b** gave a mixture of 6- and 8-methylalloxazine **8g** and **8l** (1:9) with traces of the corresponding *N*-oxides. After methylation and reduction, the mixture of regioisomers **5l** and **5g** was separated by column chromatography.

A series of truxinates **12** possessing various substituents was prepared as model substrates, in order to investigate the ability of various flavin photocatalysts to drive the corresponding oxidative [2+2] cycloeliminations. Synthesis started from cinnamic acids **13** which were transformed to anhydrides **14** with triphosgene (Scheme 4). Anhydrides were transformed into cyclobutane **15** *via* photocatalytic cycloaddition by using 7,8-dimethoxy-1,3-dimethylalloxazine (**5k**) and illumination at 400 nm.[25] The sensitized cycloaddition reaction led to the mixtures of products containing small amounts of anhydrides (*E*,*Z*)-**14** and (*Z*,*Z*)-**14**, which were formed by isomerization of **14**, isomeric cyclobutane (*anti-trans* product), and the major product **15**. Cyclobutane anhydrides **15** were typically obtained as oils and used without purification, due to their instability on silica. Thus, **15** were hydrolyzed to acids and transformed *via* dichloride into esters **12**. The final ester products **12** were purified by column chromatography, which allowed its separation from the monomer esters and the minor cyclobutane esters **16**, as side products. The synthesis of the other cyclobutane substrates **17–24** is described in the ESI.

Spectral and electrochemical properties

All salts **2** absorb blue light with absorption maxima for the $S_1 \leftarrow S_0$ transition ranging from 424 to 479 nm (see Figure S19). While the monomethoxy derivatives **2h** and **2i** absorb more in

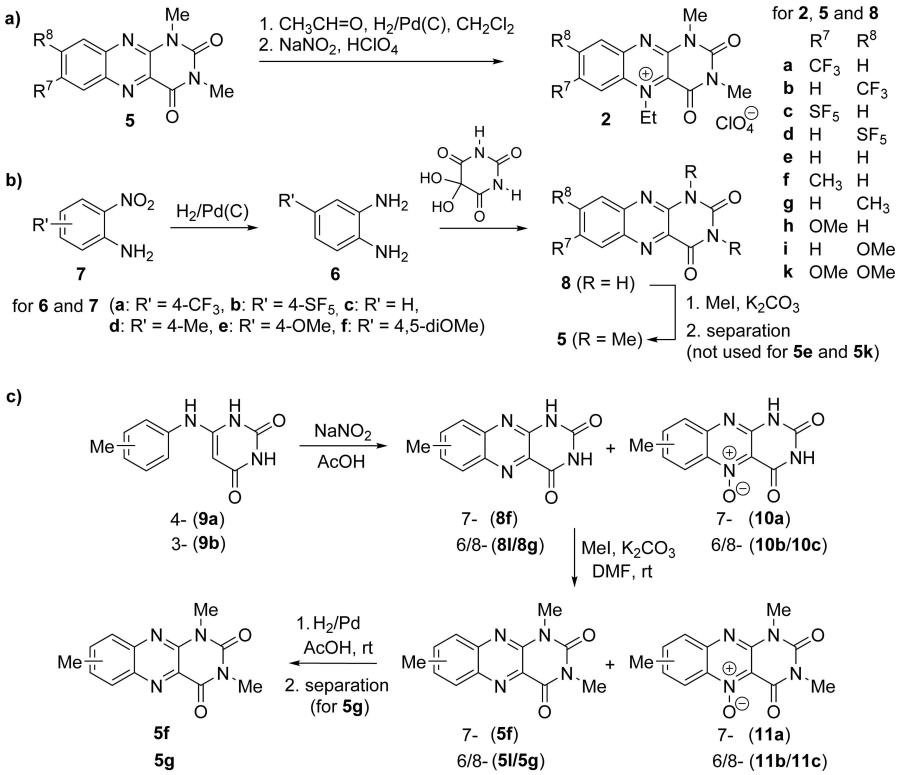

Scheme 3. Synthesis of flavinium salts **2** (**a**) and synthetic approaches towards flavins **5** (**b**, **c**).

© 2020 The Authors. ChemPlusChem published by Wiley-VCH GmbH

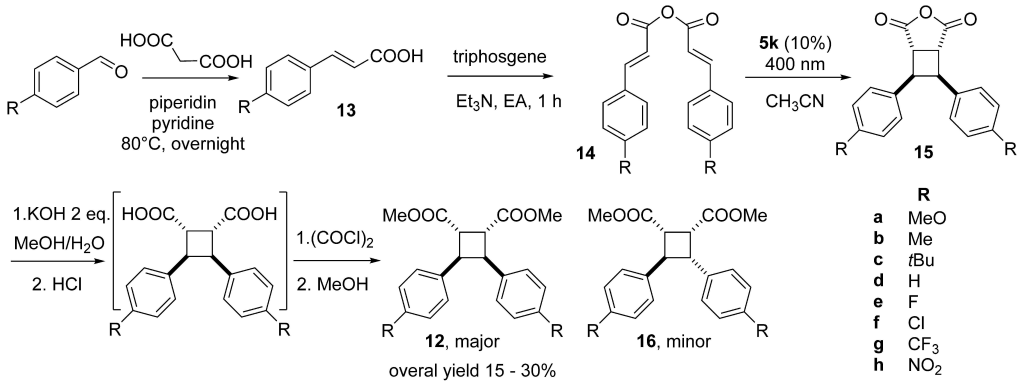

Scheme 4. Synthesis of truxinates **12**.

the blue part of this range, the dimethoxy derivative **2k** absorbs in the reddest part of this range (see Table 2 and Figure S19). The emission maxima of the salts **2** for the $S_1 \rightarrow S_0$ transition lie in the range from 525 to 540 nm with the exception of **2f**, **2h**, and **2i** with maxima at 550, 586, and 589 nm, respectively. In contrast to the alloxazinium salts the alloxazines have blue shifted absorption maxima for the $S_1 \leftarrow S_0$ transition in the range of 372 to 424 nm. The corresponding emission maxima range from 426 to 475 nm (see Table 3).

The quaternization of the alloxazines **5** resulting in the salts **2** strongly influenced their redox properties as observed by significant shifts of the first reduction potential by *ca.* 0.7 V. The substitution in positions 7 and 8 for both series of salts and neutral alloxazines changed the reduction potential by *ca.* 0.3 V. The redox properties of the excited singlet state $E^*(S_1)$ can be determined from the Rehm-Weller equation,[26] which are summarized in Tables 2 and 3. However, the oxidation power should be smaller, since the cycloelimination is initiated *via* the triplet state of the flavinium catalyst. For instance, $E^*(T_1)$ for **2b** was calculated quantum chemically to 2.20 V.

Table 2. Spectroscopic and electrochemical data for flavinium salts **2**.

Flavinium salt	λ_{abs} [nm][a]	λ_F [nm][b]	E° (1) [V][c]	E^{0-0} [eV][d]	E^* [V][e]
2a	442	525	0.01	2.56	2.57
2b	450	528	0.02	2.54	2.56
2c	442	528	0.02	2.56	2.58
2d	450	526	0.04	2.54	2.58
2e	451	535	−0.10	2.52	2.42
2f	463	550	−0.09	2.45	2.36
2g	447	533	−0.09	2.53	2.44
2h	424	586	−0.14	2.46	2.32
2i	425	589	−0.07	2.45	2.38
2k	479	540	−0.28	2.54	2.26

[a] Lowest energy band in the absorption spectra. [b] The maximum of the fluorescence emission spectrum when excited at λ_{abs}. [c] First reduction wave *vs.* SCE (reversible). [d] Approximated from absorption and emission maxima; [e] Excited state reduction potential $E^* = E^\circ + E^{0-0}$ (ref. [26]).

Table 3. Spectroscopic and electrochemical data for alloxazines **5**.

Alloxazine	λ_{abs} [nm][a]	λ_F [nm][b]	E° (1), [V][c]	E^{0-0} [eV][d]	E^* [V][e]
5a	380	426	−0.72	3.08	2.36
5b	373	432	−0.71	3.08	2.37
5c	374	428	−0.33	3.10	2.77
5d	382	440	−0.43	3.02	2.59
5e	378	435	−0.96	3.05	2,09
5f	376	429	−0.88	3.08	2.20
5g	388	447	−0.84	2.97	2.13
5h	424	475	−0.91	2.76	1.85
5i	372	475	−0.9	2.92	2.02
5k	391	442	−1.05	2.98	1.94

[a] Lowest energy band in the absorption spectra. [b] The maximum of the fluorescence emission spectrum when excited at λ_{abs}. [c] First reduction wave *vs.* SCE (reversible). [d] Approximated from absorption and emission maxima. [e] Excited state reduction potential $E^* = E^\circ + E^{0-0}$ (ref. [26]).

Cycloeliminations

The cycloelimination mediated by various alloxazinium salts **2** was investigated for a series of truxinates **12** with the oxidation potential tuned by the substitution in position 4- of its phenyl groups (Table 4). For the methyl derivative **12b** next to the cycloreversion also significant side reactions were observed that most probably arose from benzyl radical formation leading to a methyl group transformation. Very electron deficient substrates **12g** and **12h** (not shown in Table 4) with a CF_3 or NO_2 group,

Table 4. Cycloreversion by salts **2**.

Catalyst	Substrate[a] (E_{ox}[V])					
	12a[b] (1.5)	**12c**[b] (1.8)	**12d**[c] (2.1)	**12f**[c] (> 2.2)	**12g**[c] (> 2.2)	**3a**[b] (2.05)
2a	72	72	8	11	0	quant.
2b	67	86	22	12	0	92
2c	22	78	13	5	0	70
2d	23	93	24	0	0	55
2e	100	100	23	13	0	trace
2f	59	52	9	0	0	0
2g	22	58	9	0	0	5
2h	80	76	10	0	0	0
2i	83	68	13	0	0	0
2k	100	100	5	10	0	quant.

[a] Substrate (0.02 mmol), **2** (2.5 mol%), acetonitrile (1 mL), 450 nm, room temperature, under Ar atmosphere. [b] 10 min. [c] 60 min.

© 2020 The Authors. ChemPlusChem published by Wiley-VCH GmbH

respectively, were not opened with salts **2**. In contrast, electron-enriched truxinates **12a** and **12c** with a methoxy or *tert*-butyl group were opened by all salts **2** with high conversion within 10 minutes. The substrates **12d** and **12f** with oxidation potentials between 2.0 V and 2.2 V were opened with electron-deficient alloxazinium salts **2a**–**d**, however, a prolonged reaction time (60 min) was necessary to achieve significant conversions. Interestingly, cycloelimination of **12d** and **12f** occurred also with the unsubstituted salt **2e** and with the electron-enriched dimethoxy derivative **2k**. Analogous results were also obtained for the coumarin dimer **3a** which was effectively opened with **2a**–**d** and **2k** after 10 min.

Further, the performance of the dimethoxy derivative **2k** in comparison to **2b** for a series of substrates was investigated both on an analytical and preparative scale (Table 5). Although, **2k** compared to **2b** has lower oxidation properties in terms of the excited state reduction potential (see Table 2), comparable efficiencies on cycloeliminations were obtained for both photocatalysts. Both, **2k** and **2b**, split the coumarin dimer **3a** (Entry 1), the cyclic coumarin aza-analogue **3b** (Entry 2), the

Table 5. Comparison of cycloreversion mediated by either **2b**[14] or **2k** using selected cyclobutane derivatives.

Entry	Cyclobutane	E^{ox} [V][c]	Product	λ_{exc} [nm]	Catalyst	Analytical scale[a]		Preparative scale[b]	
						Time [min]	conv.[d] [%]	Time [min]	Yield[e] [%]
1	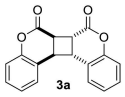 **3a**	2.05	 **4a**	450	2b	10	quant.	30	92
				450	2k	10	quant.	30	93
				530	2b	60	85	–	–
				530	2k	480	quant.	–	–
2	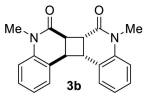 **3b**	1.34	 **4b**	450	2b	10	quant.	30	88
				450	2k	10	quant.	30	91
3	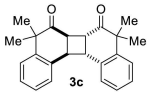 **3c**	2.14	 **4c**	450	2b	60	39[f]	240	52
				450	2k	60	6	–	–
4	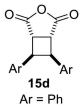 **15d** Ar = Ph	> 2.2	 **14d**	450	2b	60	0	–	–
				450	2k	60	0	–	–
5	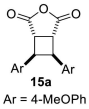 **15a** Ar = 4-MeOPh	1.71	 **14a**	450	2b	10	quant.	10	86
				450	2k	10	quant.	10	83
6	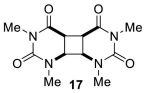 **17**	1.77	 **25**	450	2b	10	quant.	10	91
				450	2k	10	80	10	86
7	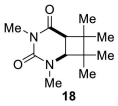 **18**	1.55	 **25** +	450	2b	60	quant[f]	120	75
				450	2k	60	71	60	87
8	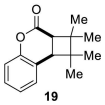 **19**	2.02	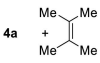 **4a** +	450	2b	60	47	60	50
				450	2k	60	45	60	57
9	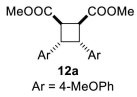 **12a** Ar = 4-MeOPh	1.57	 **26** Ar = 4-MeOPh	450	2b	10	quant.	10	94
				450	2k	10	quant.	10	92
10	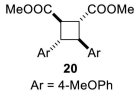 **20** Ar = 4-MeOPh	1.73	 **26** Ar = 4-MeOPh	450	2b	60	7[f]	–	–
				450	2k	60	quant.	60	78
11	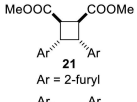 **21** Ar = 2-furyl	1.69	 **27** Ar = 2-furyl	450	2b	10	quant.	10	86
				450	2k	10	quant.	10	91
12	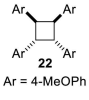 **22** Ar = 4-MeOPh	1.35	 **28** Ar = 4-MeOPh	450	2b	10	78	10	88[g]
				450	2k	10	quant.	10	94

[a] Substrate (0.02 mmol), **2b** or **2k** (2.5 mol%), acetonitrile (1 mL), room temperature, under Ar atmosphere. [b] Substrate (0.4 mmol), **2b** or **2k** (5 mol%), acetonitrile (20 mL), room temperature, under Ar atmosphere. [c] Values *vs.* SCE. [d] Conversions from ^{1}H NMR. [e] Yield of isolated product. [f] 10 mol% of **2**. [g] Contained 10% of *Z*-isomer.

© 2020 The Authors. ChemPlusChem published by Wiley-VCH GmbH

cyclic anhydride **15a** (Entry 5), the model of the thymine dimer **17** (Entry 6), the cycloadducts with tetramethylethylene **18** and **19** (Entries 7 and 8), the truxilate **12a** (Entry 9), its sensitive furan-containing analogue **21** (Entry 11), and the *cis*, *trans*-isomer of tetrakis(4-methoxyphenyl)cyclobutane **22** (Entry 12). The dimer **3c** is only opened with **2b**, however, a prolonged reaction time is needed. The cyclic anhydride **15d** with non-substituted phenyl rings is beyond the limit of both flavinium photocatalysts, which is in line with its high oxidation potential (Entry 4).

Substrate **20** (all-*trans* isomer of **12a**; Entry 10) needed a prolonged irradiation time, although it has a relatively low oxidation potential. This can be explained by a missing *cis*-effect[27] (see below for further details). Since salt **2b** photodecomposes (see first section) only a low cycloelimination yield of **20** could be achieved even with a high catalyst loading up to 10%. In contrast, the photostable **2k** splits **20** effectively.

The different photostability of **2b** and **2k** is also reflected in the course of the cyclobutane **18** photocycloelimination, which has no high oxidation potential, but is still relatively difficult to split for both photocatalysts (Figure 5). The conversion rate for the splitting of **18** into **25** in case of **2b** is initially fast but stops after several minutes at a level of *ca.* 70% indicating a significant decomposition of **2b** (black line in Figure 5). In contrast, the cycloelimination of **18** using **2k** is throughout significantly slower, but is quantitative within 60 minutes (red line in Figure 5) indicating a negligible photodecomposition of **2k** on this time scale. Further, the reusability of **2b** and **2k** was investigated for the model reaction with **3a**, which is split quantitatively by both photocatalysts. While **2k** could be used several times, **2b** could only be used once due to photodecomposition (Table 6).

In the absence of any substrate only **2k** showed significant photostability. **2b** was decomposed completely already after 2 min of irradiation, while only *ca.* 10% of **2k** decomposed after 60 min of irradiation under identical conditions (see ESI for more details). Therefore, the dimethoxyalloxazinium salt **2k** with its sufficiently high redox potential for oxidative splitting of most substrates in combination with its high photostability represents a valuable photocatalyst for cycloeliminations.

Finally, we noticed a significant influence of the substrate configuration on the cycloelimination rate, known as the *cis*-effect,[27] *i.e.* an acceleration of the cyclobutane splitting due to steric repulsion between neighboring substituents in *cis*-position, *e.g.* mainly phenyl rings. This was already shown on the compounds **12a** and **20**. Interestingly, using **2k** even the cycloelimination of the all-*trans* derivative **20** is observed. Furthermore, cycloelimination of the other *trans*-diarylcyclobutanes without aryl group repulsion could be split by **2k** (Table 7), although less efficient compared with their *cis*-derivatives.

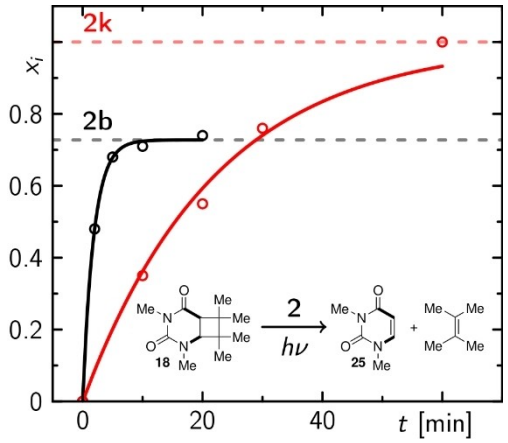

Figure 5. Course of photocycloelimination of **18** mediated by **2b** and **2k**.

Table 6. Consecutive photocycloelimination experiments with **2b** and **2k** on the model substrate **3a** forming **4a**.[a]

Entry	Cat.	Conv. [%] 1st round	2nd round	3rd round
1	**2b**	100	0	–
2	**2k**	100	100	75

[a] Substrate **3a** (0.02 mmol), **2b** or **2k** (2.5 mol%), acetonitrile (1 mL), λ_{exc} = 450 nm, room temperature, under Ar atmosphere; 10 minutes each round.

Cycloaddition vs. cycloelimination

The neutral dimethoxyalloxazine **5k** was described as a useful mediator of intramolecular [2+2] photocycloadditions *via* energy transfer.[25] Thus, we speculated, whether the corresponding alloxazinium perchlorate **2k** could also trigger this reaction. Indeed, **2k** catalyzes the [2+2] cycloaddition of selected anhydrides **14** similarly to the neutral alloxazine **5k** (Table 8). Almost all tested cinnamic anhydrides **14** were transformed to cyclobutanes **15** with high stereoselectivity in moderate to quantitative yields in acetonitrile with **2k** (it should be noted that only the cyclobutane products with *anti*/*cis* configuration were observed). Only for anhydride **14a** (Table 8, Entry 1) no formation of its cycloadduct was observed, which may be explained by a **2k**-initiated oxidative cycloelimination of **15a** back to **14a** which is faster compared to the formation of **15a** (Scheme 5a). In contrast, oxidative cycloelimination of **15c**, **15d**, **15f** and **15g** with **2k** was not observed in agreement with their too high oxidation potentials as shown above (cf Table 5, Entry 4).

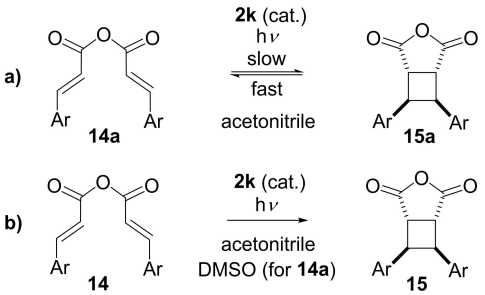

Scheme 5. Cycloaddition/cycloelimination in the **14**/**15** system mediated by **2k** and irradiation at 450 nm. For conversions and conditions, see Table 8.

© 2020 The Authors. ChemPlusChem published by Wiley-VCH GmbH

Table 7. Cycloreversion of *cis*- and *trans*-diarylcyclobutanes mediated by **2k**.[a]

Entry	Time [min]	*cis*-isomer	Conv. [%][b]	*trans*-isomer	Conv. [%][b]
1	10	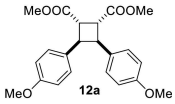 **12a**	quant.	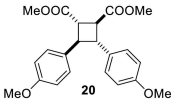 **20**	5
2	1	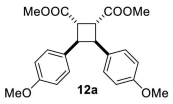 **12a**	37	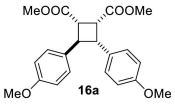 **16a**	6
3	10	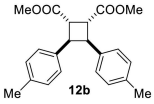 **12b**	quant.	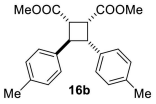 **16b**	40
4	10	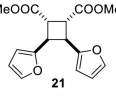 **21**	quant.	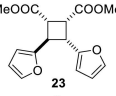 **23**	32
5	10	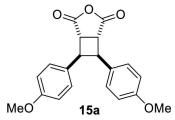 **15a**	quant.	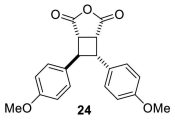 **24**	15

[a] Substrate (0.02 mmol), **2k** (2.5 mol%), acetonitrile (1 mL), $\lambda_{exc} = 450$ nm, room temperature, under Ar atmosphere. [b] Conversions from ^{1}H NMR.

Table 8. [2+2] Cycloadditions of anhydrides **14** sensitized by **2k**.[a]

Entry	Anhydride	Product	Time [min]	Conv.[b] [%]
1	 **14a** Ar = 4-MeOPh	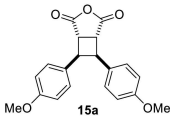 **15a**	10	0
2	 **14c** Ar = 4-*t*BuPh	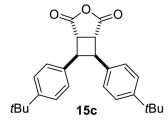 **15c**	10/60	70/46
3	 **14d**	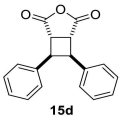 **15d**	10/60	100/50
4	 **14f** Ar = 4-Cl	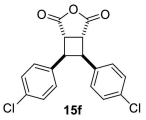 **15f**	60	76
6	 **14g** Ar = 4-CF_3	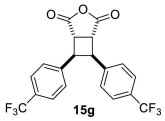 **15g**	60	42

[a] Substrate (0.02 mmol), **2k** (2.5 mol%), acetonitrile (1 mL), $\lambda_{exc} = 450$ nm, room temperature, under Ar atmosphere. [b] Conversions from ^{1}H NMR.

The cycloelimination is only efficient in acetonitrile or nitromethane.[14] In contrast, the cycloaddition does not depend on the solvent significantly (cycloadditions with alloxazines work well in dimethylsulfoxide, dimethylformamide, alcohols, acetone, toluene, chlorinated solvents, and best in acetonitrile).[25a] In order to avoid the cycloelimination we selected dimethylsulfoxide as a suitable solvent for the cycloaddition of **14a** with 2.5% of **2k**. Indeed, under these conditions 89% of cyclobutane **15a** were formed after 10 minutes of irradiation (Scheme 5b).

Conclusion

We described the detailed mechanism of the [2+2] photocycloelimination of the coumarin dimer **3a** as a model substrate mediated by the salt **2b**. After photoexcitation, **2b** forms efficiently its triplet state, *i.e. ca.* 89%, in which it can abstract an electron from a substrate (dimer) initiating the cyclobutane ring opening to form the final product coumarin (**4a**) partly *via* its radical cation $\mathbf{4a}^{\bullet+}$ and oxidizing $\mathbf{2b}^{\bullet+}$ back to **2b**. Depending on the concentration conditions the conversion is also accelerated by an additional radical chain mechanism.

Simultaneously, it turned out that **2b** undergoes fast dealkylation forming the relatively photostable neutral alloxazine **5b** which also drives the cycloelimination, however, with a two orders of magnitude lower quantum yield. Despite its strong oxidizing properties, the lower stability of the electron deficient salt **2b** as well as its tendency to form the pseudobase **2b**–**OH** by reaction with water, *e.g.* due to residual moisture in the solvent, can limit its practical applications in photocatalysis.

The photocycloelimination was tested for various differently substituted alloxazinium salts **2** on the conversion of the coumarin dimer **3a** and on a series of truxinates **12**. The 7,8-dimethoxyalloxazinium derivative **2k** showed a similar efficiency as the 8-trifluoromethyl analogue **2b**. Importantly, the flavinium salt **2k** is very photostable allowing the cycloelimination to proceed to high conversions even for substrates whose opening requires to overcome a high activation barrier due to steric hindrance as in cyclobutane **20**. Additionally, **2k** also

© 2020 The Authors. ChemPlusChem published by Wiley-VCH GmbH

initiates the intramolecular [2+2] cycloaddition of electron deficient and electron neutral cinnamic anhydrides **14** which do not undergo back oxidative cycloelimination because of their high oxidation potential. With 4-methoxycinnamic anhydride **14a**, both cycloaddition to **15a** and its back cycloelimination to **14a** occur in the presence of **2k**. Interestingly, the preference of either the cycloelimination or cycloaddition product of this reversible process mediated by a single catalyst can be tuned by the solvent environment.

To our knowledge this is the first example of a detailed investigation of positively charged flavin derivatives as photocatalysts. The most promising flavinium catalyst for photooxidative processes turned out to be **2k**, and our findings demonstrate also its potential for broader applications in various other photocatalytic transformations.

Experimental Section

General comments to the starting material and synthesis

Starting materials and reagents were obtained from commercial suppliers and used without further purification. The solvents were purified and dried using standard procedures.[28] Flavinium salts **2**, alloxazines **5**, and substrates **12**–**22** were prepared and characterized as described in the ESI. **NMR spectra** were recorded on a Varian Mercury Plus 300 (299.97 MHz for ^{1}H, 75.44 MHz for ^{13}C, and 282.23 MHz for ^{19}F) or Agilent 400-MR DDR2 (399.94 MHz for ^{1}H and 100.58 MHz for ^{13}C) at 298 K unless otherwise stated. Chemical shifts δ are given in ppm, using residual solvent or tetramethylsilane as an internal standard. Coupling constants *J* are reported in Hz. High-resolution **mass spectra** were obtained on Q-Tof Micro (Waters), equipped with a quadrupole and time-of-flight (TOF) analyser and subsequent a multichannel plate (MCP) detector. Thin layer chromatography (TLC) analyses were carried out on a DC Alufolien Kieselgel 60 F254 (Merck). Preparative column chromatography separations were performed on a silica gel Kieselgel 60 0.040–0.063 mm (Merck). **Melting points** were measured on a Boetius melting point apparatus and are uncorrected.

General procedures for cycloelimination reaction

Experiments on analytical scale: The cyclobutane derivative (0.02 mmol) and the alloxazinium salt **2** or alloxazine **5** (0.5 μmol) were placed in a Schlenk tube and anhydrous acetonitrile (1 mL) was added. The homogenous solution was deoxygenated three times *via* the freeze-pump-thaw technique. The solution in the Schlenk tube was irradiated (LED, Luxeon STAR/0, 1030 mW@700 mA, 450 nm for **2** or LED, LED Engin LZC-70UA00 400 nm for **5**) for a certain time, usually for 10 minutes. The reaction mixture was analyzed by ^{1}H NMR.

Experiments on preparative scale: The cyclobutane derivative (0.4 mmol) and the alloxazinium salt **2** (**2b** or **2k**; 0.02 mmol) were placed in a Schlenk tube and anhydrous acetonitrile (20 mL) was added. The homogenous solution was deoxygenated three times *via* the freeze-pump-thaw technique. The solution in the Schlenk tube was irradiated (6×LED, Luxeon STAR/0, 1030 mW@700 mA, 450 nm for **2** or 6×LED, LED Engin LZC-70UA00 400 nm for **5**) for a certain time depending on the cyclobutane substrate. After irradiation, the solvent was removed, and the crude product was purified by column chromatography (see ESI for details and products characterization).

Electrochemical measurements

Electrochemical measurements were performed using a standard three-electrode system in a methrom type electrochemical cell with a glassy carbon working electrode, silver wire pseudo-reference electrode, and a platinum wire auxiliary electrode.[16d,17a] Cyclic voltammograms were collected by PGSTAT128 N. The cyclic voltammetry measurements were carried out in acetonitrile containing a cyclobutane or alloxazinium salt **65** ($c = 1\times10^{-3}$ mol L^{-1}) and tetrabutylammonium hexafluorophosphate ($c = 1\times10^{-1}$ mol L^{-1}) as supporting electrolyte under argon atmosphere. The scan rate was 100 mV s^{-1}. The measured redox potentials were converted into values relative to the standard calomel electrode (SCE) using the standard redox couple Fc^{+}/Fc as suggested by Addison and others.[29] Conversion of the measured values into those *vs.* SCE involved subtraction of the difference between experimental $E_{1/2}$ values for the standard redox couple Fc^{+}/Fc measured after each experiment (relative to the Ag wire) and $E_{1/2}$ value for the standard redox couple Fc^{+}/Fc measured against SCE at the same apparatus (+0.381 V, the value obtained as an average of 5 measurements).

Stationary UV/Vis absorption and emission spectroscopy

All UV/Vis absorption (Agilent Cary 60 or Shimadzu UV-1800 spectrophotometer) and UV/Vis emission spectra (Varian Cary Eclipse or Jobin Yvon Fluorolog-3 fluorescence spectrofluorometer) were recorded at room temperature. Fluorescence quantum yields were determined with a Hamamatsu C9920-02 system equipped with a Spectralon integrating sphere. The quantum yield accuracy is < 10 % according to the manufacturer.

Stepwise illumination and recording of UV/Vis absorption spectra

The relative product quantum yield (PQY) in the presence of molecular oxygen was determined by recording absorption spectra of a particular system after step-wise temporally and geometrically defined illumination (pulse width $\Delta t = 1$ s, $\lambda_{exc} = 390/460$ nm) in 10×10 mm quartz cell filled with 3 mL sample that was continuously stirred when the sample was illuminated. These sequences of spectra showing the product build-up upon illumination were decomposed into the contributing species spectra and corresponding concentration-time profiles (see ESI for all data). The initial slope of the product build-up over illumination time is proportional to the product quantum yield. For comparison within all measurements the illumination times where corrected by the corresponding overlap integrals between the normalized spectrum of the excitation source and the absorption spectrum of the corresponding chromophore, that was excited. The absolute quantum yield was calculated from recording also the product formation of the known photo-oxidation of 4-methoxybenzylic alcohol (MBA) to the corresponding aldehyde by tetra-acetyl riboflavin (TARF) as a reference system with a known quantum yield.[21a]

Time-resolved UV/Vis emission spectroscopy

A self-constructed Time Correlated Single Photon Counting (TCSPC) setup[16h,30] was used to record emission decay data at single detection wavelength. A quartz cuvette with four optical windows of the dimension 2 mm×10 mm was used. The sample was excited along the 2 mm pathlength and the emission was recorded orthogonally to this. The optical density of the sample was set to *ca.* 0.1 at the excitation wavelength over 2 mm pathlength.

© 2020 The Authors. ChemPlusChem published by Wiley-VCH GmbH

Time-resolved UV/Vis absorption spectroscopy

The ns to ms transient absorption spectroscopy was recorded by a streak camera setup as described previously.[16h,21a,30–31] In brief, the third harmonic of a Nd:YAG laser (10 Hz, Surelite II, Continuum) pumping an Optical Parametric Oscillator (OPO, Continuum) tuned to 355/460 nm (10 mJ, *ca.* 10 ns) was used for sample excitation. As a probe light a pulsed 150 W Xe-flash lamp (Applied Photophysics) was used which was focused three times *via* toric mirror optics: i) before probe shutter, ii) into sample, iii) into spectrograph. The entire white light probe pulse was analyzed by a combination of a spectrograph (200is, Bruker) and a streak camera (C7700, Hamamatsu Photonics). The use of mechanical shutters enabled the recording of a sequence of three individual data sets: i) an image (D_{FL}) with both flash lamp and laser, ii) an image (D_0) without any incoming light, and iii) an image (D_F) only with the flash lamp. 100 of such sequences were recorded and corresponding data sets were averaged. Then, the TA was calculated as [Eq. (1)]:

$$\Delta OD = \log\left(\frac{D_F - D_0}{D_{FL} - D_0}\right) \quad (1)$$

A 10 mL sample was stepwise cycled by a peristaltic pump (ecoline, ISMATEC) through a flow cell with a pathlength of 2 mm for pump and 10 mm for probe beams (dimensions: 2 mm × 10 mm × 30 mm, Starna) ensuring a total replacement of the sample prior to each individual measurement. No photocatalyst degradation was observed under the used conditions.

The Sub-ps Pump/Supercontinuum-Probe Spectroscopy were carried out using UV/Vis pump-supercontinuum probe spectrometer at 1 kHz repetition frequency as described in ref.[16h] In brief, a Ti-sapphire amplifier system (Coherent Libra) was used to generate 800 nm with 1.2 mJ pulses at 1 kHz. The output was split into three parts of which only two were used: 1) *Ca.* 50% of the 800 nm pulses were used to pump a colinear Optical Parametric Amplifier (OPA, TOPAS-800-fs, Light Conversion) tuned to pump pulses centered at *ca.* 450 nm (*ca.* 100 fs, *ca.* 400 nJ at the sample position) for sample excitation. 2) *Ca.* 10% were used to pump a non-colinear Optical Parametric Amplifier (NOPA, In-house build) tuned to pulses centered at *ca.* 530 nm (*ca.* 100 fs, *ca.* 5 μJ at the CaF_2 position) for generation of supercontinuum white light probe pulses by focusing into a moving CaF_2 disc of 1 mm thickness giving a probe spectrum ranging from 310 to 700 nm. Pump pulses were delayed *via* a motorized delay line equipped with an open corner cube mirror up to 2 ns. Two complementary high-speed spectrographs (Entwicklungsbüro EB Stresing) for signal and reference recording were used. The pump and probe pulses were focused colinearly into the sample to spot sizes of *ca.* 80 μm and 60 μm full width at half maximum (FWHM), respectively. For longer delays reaching out from ns to μs time ranges a similar spectrometer was used in which the pump laser was electronically delayed relative to the probe laser. A detailed description can be found in ref.[32] The relative polarizations between the pump and probe were set by a half-wave plate in the pump-beam path to magic angle (54.71°) for observations of pure population changes. The averaged pre-t_0 laser scatter signal was subtracted from the data and the *ca.* 1 ps chirp of the white light was corrected for prior to data analysis using the coherent artefact as an indicator for time zero at each wavelength. Throughout the probe range, the spectral resolution was better than 4 nm and the temporal resolution was better than 150 fs. 10 individual scans with averaging 100 spectra per time point were typically recorded. The time axis – within total 500 points – was linear between −1 and 2 ps and logarithmic from 2 ps to the maximum time delay ensuring that the dynamics on every timescale will have equal weighting in the fitting analysis. In the sub-ps transient absorption setup 10 mL of the sample were cycled through an in-house build cell with a pathlength of *ca.* 100 μm for pump and probe beams. In the sub-ns transient absorption setup 10 mL of the sample were cycled through a flow cell (Starna) with a pathlength of 2 mm for pump and probe beams. In all cases all scans resulted in reproducible data sets. Additionally, the integrity of the sample was checked by recording stationary absorption spectra before and after each measurement. No photocatalyst degradation was observed under the used conditions. The shown data correspond to one representative measurement. No smoothing or filtering procedures were applied to the data.

Transient absorption data analysis and modelling

SVD-based rank analysis and global fitting were performed using an in-house written program described previously.[21b,30–31] In brief, the linear least squares problem in Equation (2)

$$\chi^2 = \|\Delta\mathbf{A} - \mathbf{FB}\|^2 = \text{Min} \quad (2)$$

is solved, where △**A** is the time-resolved absorption data matrix, **F** is the matrix containing the analytical functions accounting for the temporal changes in the data, *i.e.* exponential decays (convoluted with the instrument response, typically a Gaussian function), and **B** is the matrix with the to be determined spectra. Further optimization of χ^2 is achieved by optimizing the rate constants in **F** by a nonlinear least squares algorithm. As a result of such fits so-called decay associated difference spectra (DADS in matrix **B**) and their associated optimized rate constants are obtained. These are the unique result of the global fit and this treatment does not require any model for the kinetics involved in the transient processes. The number of exponentials in the global fit is determined by the SVD-based rank analysis, which is described elsewhere.[33] The model that relates the actual species kinetics to the elementary function is applied afterwards resulting in species associated spectra (SAS). The shape of the SAS in terms of identity with well-known spectra or following physical laws decides about the appropriateness of the model. This step does not change the χ^2 value found in the global fit and, therefore, this procedure has the advantage that all interpretation is performed with the same quality of fit.

As an alternative analysis, known species spectra, taken either from literature or recorded in this work, were taken in order to decompose the recorded time-resolved data matrix using the transpose of the data matrix in [Eq. (2)] and using the basis spectra instead of analytical functions. The resulting concentration-time-profiles inform about the appropriateness of the basis spectra and the physical reasonability, *i.e.* total sum of species being constant to 1.

Quantum chemical calculations

Quantum-chemical calculations on the excited singlet and triplet states of **2b** as well as on the radical species of **2b** that potentially contribute to the time-resolved absorption signals, *i.e.* **2b**$^{\bullet}$ and **2b**$^{\bullet+}$, were performed using the Firefly QC package,[34] which is partially based on the GAMESS (US)[35] source code. All ground state structures were optimized on the level of restricted open shell density functional theory (ROHF-DFT) using the B3LYP functional and the split-valence 6–31G(p,d)$^{++}$ basis set. In terms of the radical spectrum calculation, complete active space self-consistency field (CASSCF) theory was used in order to calculate the static correlation energy. The most intense electronic transitions of **2b** radicals, *i.e.* $D_X \leftarrow D_0$ are of π–π* and n–π* type. Thus, 13 contributing π

© 2020 The Authors. ChemPlusChem published by Wiley-VCH GmbH

electrons were included into the CAS, distributed over 12 molecular orbitals (MO), and energy averaging over 10 states with equal weights, *i.e.* CASSCF(13,12)10, was performed. In order to calculate the dynamic correlation energy extended multi-configuration quasi-degenerate perturbation theory (XMCQDPT) was used on top of the CASSCF optimized MOs.[36] In all cases an intruder state avoidance (ISA) denominator shift of 0.02 was used. Solvent effects were taken into account with the polarized continuum model (PCM).

Acknowledgements

This project was supported by the Czech Science Foundation (Grant No. 18-15175S). R.J.K. thanks the Deutsche Forschungsgemeinschaft for a Research Fellow stipend (KU 3190/1-1, KU 3190/2-1) supporting this project. The authors are grateful to Prof. Eberhard Riedle (BioMolekulare Optik, Ludwig-Maximillians Universität München) for allowance to use of the ns to μs transient absorption apparatus. T.H. and R.C. thank Dr. Petr Beier for providing pentafluorosulfanyl precursors.

Conflict of Interest

The authors declare no conflict of interest.

Keywords: cyclobutanes · cycloelimination reactions · electron transfer · photocatalysis · time-resolved spectroscopy

[1] a) A. Sancar, *Angew. Chem. Int. Ed.* **2016**, *55*, 8502–8527; *Angew. Chem.* **2016**, *128*, 8643–8670; b) A. Sancar, *Chem. Rev.* **2003**, *103*, 2203–2238; c) K. Brettel, M. Byrdin, *Curr. Opin. Struct. Biol.* **2010**, *20*, 693–701.
[2] a) E. Schaumann, R. Ketcham, *Angew. Chem. Int. Ed.* **1982**, *21*, 225–247; *Angew. Chem.* **1982**, *94*, 225–229; b) K. Mizuno, C. Pac, CRC Press, **1995**, pp. 358–374.
[3] a) D. Davis, V. P. Vysotskiy, Y. Sajeev, L. S. Cederbaum, *Angew. Chem. Int. Ed.* **2011**, *50*, 4119–4122; *Angew. Chem.* **2011**, *123*, 4205–4208; b) N. Paul, M. Jiang, N. Bieniek, J. L. P. Lustres, Y. Li, N. Wollscheid, T. Buckup, A. Dreuw, N. Hampp, M. Motzkus, *J. Phys. Chem. A* **2018**, *122*, 7587–7597; c) K. Shima, J. Kimura, K. Yoshida, M. Yasuda, K. Imada, C. Pac, *Bull. Chem. Soc. Jpn.* **1989**, *62*, 1934–1942.
[4] a) R. B. Woodward, R. Hoffmann, *Angew. Chem. Int. Ed.* **1969**, *8*, 781–853; *Angew. Chem.* **1969**, *81*, 797–869; b) R. Hoffmann, R. B. Woodward, *J. Am. Chem. Soc.* **1965**, *87*, 2046–2048.
[5] P. v. R. Schleyer, J. E. Williams, K. R. Blanchard, *J. Am. Chem. Soc.* **1970**, *92*, 2377–2386.
[6] a) J. Liese, N. Hampp, *J. Phys. Chem. A* **2011**, *115*, 2927–2932; b) C. Pac, *Trends Phys. Chem.* **1990**, *1*, 15–31; c) M. Yasuda, K. Yoshida, K. Shima, C. Pac, S. Yanagida, *Bull. Chem. Soc. Jpn.* **1989**, *62*, 1943–1950.
[7] a) Z. S. Kean, Z. Niu, G. B. Hewage, A. L. Rheingold, S. L. Craig, *J. Am. Chem. Soc.* **2013**, *135*, 13598–13604; b) Z. Chen, X. Zhu, J. Yang, J. A. M. Mercer, N. Z. Burns, T. J. Martinez, Y. Xia, *Nat. Chem.* **2020**, Ahead of Print; c) M. F. Pill, K. Holz, N. Preusske, F. Berger, H. Clausen-Schaumann, U. Luening, M. K. Beyer, *Chem. Eur. J.* **2016**, *22*, 12034–12039; d) M. J. Robb, J. S. Moore, *J. Am. Chem. Soc.* **2015**, *137*, 10946–10949.
[8] a) J. D. White, Y. Li, J. Kim, M. Terinek, *Org. Lett.* **2013**, *15*, 882–885; b) W. Oppolzer, *Acc. Chem. Res.* **1982**, *15*, 135–141; c) J. D. White, J. Kim, N. E. Drapela, *J. Am. Chem. Soc.* **2000**, *122*, 8665–8671; d) M. T. Crimmins, J. M. Pace, P. G. Nantermet, A. S. Kim-Meade, J. B. Thomas, S. H. Watterson, A. S. Wagman, *J. Am. Chem. Soc.* **2000**, *122*, 8453–8463; e) B. A. Boon, A. G. Green, P. Liu, K. N. Houk, C. A. Merlic, *J. Org. Chem.* **2017**, *82*, 4613–4624.
[9] a) C. Pac, T. Ohtsuki, Y. Shiota, S. Yanagida, H. Sakurai, *Bull. Chem. Soc. Jpn.* **1986**, *59*, 1133–1139; b) C. Pac, *Pure Appl. Chem.* **1986**, *58*, 1249–1256; c) T. Majima, C. Pac, H. Sakurai, *J. Am. Chem. Soc.* **1980**, *102*, 5265–5273; d) T. Majima, C. Pac, J. Kubo, H. Sakurai, *Tetrahedron Lett.* **1980**, *21*, 377–380.
[10] K. Okada, K. Hisamitsu, T. Mukai, *Tetrahedron Lett.* **1981**, *22*, 1251–1254.
[11] M. A. Miranda, M. A. Izquierdo, F. Galindo, *J. Org. Chem.* **2002**, *67*, 4138–4142.
[12] a) K. Miyake, Y. Masaki, I. Miyamoto, S. Yanagida, T. Ohno, A. Yoshimura, C. Pac, *Photochem. Photobiol.* **1993**, *58*, 631–636; b) C. Pac, K. Miyake, Y. Masaki, S. Yanagida, T. Ohno, A. Yoshimura, *J. Am. Chem. Soc.* **1992**, *114*, 10756–10762.
[13] R. Epple, T. Carell, *Angew. Chem. Int. Ed.* **1998**, *37*, 938–941; *Angew. Chem.* **1998**, *110*, 986–989.
[14] T. Hartman, R. Cibulka, *Org. Lett.* **2016**, *18*, 3710–3713.
[15] a) J. B. Metternich, R. J. Mudd, R. Gilmour, in *Photocatalysis in Organic Synthesis*, 2019 ed. (Ed.: B. König), Georg Thieme Verlag, Stuttgart, **2019**, pp. 391–404; b) B. König, S. Kümmel, E. Svobodová, R. Cibulka, in *Physical Sciences Reviews, Vol. 3*, **2018**; c) I. K. Sideri, E. Voutyritsa, C. G. Kokotos, *Org. Biomol. Chem.* **2018**, *16*, 4596–4614.
[16] a) N. P. Ramirez, B. König, J. C. Gonzalez-Gomez, *Org. Lett.* **2019**, *21*, 1368–1373; b) T. Hering, B. Mühldorf, R. Wolf, B. König, *Angew. Chem. Int. Ed.* **2016**, *55*, 5342–5345; *Angew. Chem.* **2016**, *128*, 5428–5431; c) L. M. Bouchet, A. A. Heredia, J. E. Argüello, L. C. Schmidt, *Org. Lett.* **2020**, *22*, 610–614; d) M. März, M. Kohout, T. Neveselý, J. Chudoba, D. Prukała, S. Niziński, M. Sikorski, G. Burdziński, R. Cibulka, *Org. Biomol. Chem.* **2018**, *16*, 6809–6817; e) T. Neveselý, E. Svobodová, J. Chudoba, M. Sikorski, R. Cibulka, *Adv. Synth. Catal.* **2016**, *358*, 1654–1663; f) B. Mühldorf, R. Wolf, *Angew. Chem. Int. Ed.* **2016**, *55*, 427–430; *Angew. Chem.* **2016**, *128*, 437–441; g) J. B. Metternich, R. Gilmour, *J. Am. Chem. Soc.* **2016**, *138*, 1040–1045; h) A. Graml, T. Neveselý, R.-J. Kutta, R. Cibulka, B. König, *Nat. Commun.* **2020**, *11*, 3174.
[17] It was shown that the usage of ethylene-bridged flavinium salts allow aerobic photooxidations of benzylic substrates, see: a) J. Zelenka, E. Svobodová, J. Tarábek, I. Hoskovcová, V. Boguschová, S. Bailly, M. Sikorski, J. Roithová, R. Cibulka, *Org. Lett.* **2019**, *21*, 114–119; b) J. Zelenka, R. Cibulka, J. Roithová, *Angew. Chem. Int. Ed.* **2019**, *58*, 15412–15420; c) A. H. Tolba, F. Vávra, J. Chudoba, R. Cibulka, *Eur. J. Org. Chem.* **2020**, *2020*, 1579–1585.
[18] a) T. Sakai, T. Kumoi, T. Ishikawa, T. Nitta, H. Iida, *Org. Biomol. Chem.* **2018**, *16*, 3999–4007; b) R. Cibulka, *Eur. J. Org. Chem.* **2015**, *2015*, 915–932; c) H. Iida, Y. Imada, S. I. Murahashi, *Org. Biomol. Chem.* **2015**, *13*, 7599–7613.
[19] a) W. J. H. Van Berkel, N. M. Kamerbeek, M. W. Fraaije, *J. Biotechnol.* **2006**, *124*, 670–689; b) F. G. Gelalcha, *Chem. Rev.* **2007**, *107*, 3338–3361.
[20] a) P. Ménová, H. Dvořáková, V. Eigner, J. Ludvík, R. Cibulka, *Adv. Synth. Catal.* **2013**, *355*, 3451–3462; b) Y. Imada, H. Iida, S. Ono, Y. Masui, S.-I. Murahashi *Chem. Asian J.* **2006**, *1*, 136–147; c) A. A. Lindén, N. Hermanns, S. Ott, L. Krüger, J.-E. Bäckvall, *Chem. Eur. J.* **2005**, *11*, 112–119; d) P. Ménová, R. Cibulka, *J. Mol. Catal. A* **2012**, *363–364*, 362–370.
[21] a) U. Megerle, M. Wenninger, R.-J. Kutta, R. Lechner, B. Konig, B. Dick, E. Riedle, *Phys. Chem. Chem. Phys.* **2011**, *13*, 8869–8880; b) R. J. Kutta, N. Archipowa, N. S. Scrutton, *Phys. Chem. Chem. Phys.* **2018**, *20*, 28767–28776.
[22] C. Franco, J. Olmsted, *Talanta* **1990**, *37*, 905–909.
[23] Y. Arakawa, T. Oonishi, T. Kohda, K. Minagawa, Y. Imada, *ChemSusChem* **2016**, *9*, 2769–2773.
[24] Y. Sakuma, S. Matsumoto, T. Nagamatsu, F. Yoneda, *Chem. Pharm. Bull.* **1976**, *24*, 338–341.
[25] a) V. Mojr, E. Svobodová, K. Straková, T. Neveselý, J. Chudoba, H. Dvořáková, R. Cibulka, *Chem. Commun.* **2015**, *51*, 12036–12039; b) V. Mojr, G. Pitrová, K. Straková, D. Prukała, S. Brazevic, E. Svobodová, I. Hoskovcová, G. Burdziński, T. Slanina, M. Sikorski, R. Cibulka, *ChemCatChem* **2018**, *10*, 849–858; c) M. Jirásek, K. Straková, T. Neveselý, E. Svobodová, Z. Rottnerová, R. Cibulka, *Eur. J. Org. Chem.* **2017**, *2017*, 2139–2146.
[26] D. Rehm, A. Weller, *Ber. Bunseng. Phys. Chem.* **1969**, *73*, 834–839.
[27] a) N. Yonezawa, T. Yoshida, M. Hasegawa, *J. Chem. Soc. Perkin Trans. 1* **1983**, 1083–1086; b) C. Pac, T. Ohtsuki, Y. Shiota, S. Yanagida, H. Sakurai, *Bull. Chem. Soc. Jpn.* **1986**, *59*, 1133.
[28] D. D. Perrin, *Purification of Laboratory Chemicals*, 4th Ed., Elsevier Science Ltd., Oxford, **1996**.
[29] H. G. Roth, N. A. Romero, D. A. Nicewicz, *Synlett* **2016**, *27*, 714–723.
[30] R. J. Kutta, Blitzlichtphotolyse – Untersuchung zu LOV-Domänen und photochromen Systemen, Universität Regensburg **2012**.

© 2020 The Authors. ChemPlusChem published by Wiley-VCH GmbH

[31] a) R.-J. Kutta, T. Langenbacher, U. Kensy, B. Dick, *Appl. Phys. B* **2013**, *111*, 203–216; b) B. Dick, U. Kensy, R.-J. Kutta, in *15 Transient Absorption*, De Gruyter, **2013**, p. 295.
[32] B. Baudisch, Time resolved broadband spectroscopy from UV to NIR, Ludwig-Maximilians-Universität München **2018**.
[33] K. Lanzl, M. v. Sanden-Flohe, R.-J. Kutta, B. Dick, *Phys. Chem. Chem. Phys.* **2010**, *12*, 6594–6604.
[34] A. A. Granovsky, **1997**, p. http://classic.chem.msu.su/gran/firefly/index.html.
[35] M. W. Schmidt, K. K. Baldridge, J. A. Boatz, S. T. Elbert, M. S. Gordon, J. H. Jensen, S. Koseki, N. Matsunaga, K. A. Nguyen, S. Su, T. L. Windus, M. Dupuis, J. A. Montgomery, Jr., *J. Comput. Chem.* **1993**, *14*, 1347–1363.
[36] A. A. Granovsky, *J. Chem. Phys.* **2011**, *134*, 214113.

Manuscript received: December 1, 2020
Revised manuscript received: December 22, 2020
Accepted manuscript online: December 23, 2020

© 2020 The Authors. ChemPlusChem published by Wiley-VCH GmbH